Int J Adv Manuf Technol (2015) 79:1645–1658
DOI 10.1007/s00170-015-6942-4

ORIGINAL ARTICLE

Laser-assisted milling of Ti-6Al-4V with the consideration of surface integrity

G. K. Hedberg · Y. C. Shin · L. Xu

Received: 18 October 2014 / Accepted: 20 February 2015 / Published online: 7 March 2015

Abstract Titanium alloys are well known for their excellent strength-to-weight ratio and corrosion resistance and is highly sought after in the aerospace industry. This study focused on experimental evaluation of laser-assisted milling (LAML) of a Ti-6AL-4V (Ti-64) workpiece which uses localized preheating of the workpiece by a laser and characterizes the improvements to the machinability of these metals. The benefits of LAML are quantified for laser parameters which are shown to maintain final surface integrity of the heat-treatable workpiece after the machining process. Laser parameters are determined based on temperature prediction modeling. Laser preheating is shown to reduce cutting force during the machining process. Machinability improvement is characterized through inspection of flank wear on the cutting tool using LAML and traditional machining methods and comparing total tool life. Systematic characterization of samples is performed using hardness measurements, scanning electron microscopy (SEM), and X-ray diffraction (XRD) to ensure that material properties remained unaltered as a result of laser preheating. An economic analysis is performed for LAML to characterize the improvement obtained despite the additional costs associated with the laser equipment.

Keywords Laser-assisted milling · Thermal analysis · Finite element · Surface integrity · Tool wear

G. K. Hedberg · Y. C. Shin (✉)
Center for Laser Based Manufacturing, School of Mechanical Engineering, Purdue University, West Lafayette, IN 47907, USA
e-mail: shin@ecn.purdue.edu

L. Xu
The Boeing Company, P.O. Box 3707, MC 5A-08, Seattle, WA 98124-2207, USA

1 Introduction

One material that continues to see applications for improved part performance is titanium. This material provides unique benefits and increased application as a result of its material properties. Titanium alloys have high strength-to-weight ratios and are very corrosion resistant. Ti-6Al-4V (Ti-64), grade 5, is an alloy that is used in the aerospace industry to provide strong, light weight components that will avoid corrosion when attached to other materials [1, 2]. The properties that make titanium alloys attractive for various applications also make these materials difficult to machine at room temperature due to excessive tool wear.

Many investigations have been conducted to study how advances in machining technologies such as tool materials, coating technology, and lubrication can improve titanium alloy machining [3–5]. Early and current studies have emphasized using traditional coolants to reduce friction and lower temperatures in the cutting zone. Many studies compared use of traditional coolant methods with other methods, such as a high pressure coolant [6, 7] and minimum quantity lubrication (MQL) techniques [8–10]. Varying degrees of success have been achieved when applying such techniques to Ti-64 alloys.

Despite the large amount of research to improve the machining speed of titanium alloys, true high-speed machining of titanium has yet to be realized. As the demands for titanium alloys have increased in recent years, new methods of material removal are needed. Thermally assisted machining is one technique that has been ascertained to increase productivity by preheating the workpiece or cooling the cutting tool.

Laser-assisted material processing is one of the emerging fields in advanced manufacturing, and research has been performed to apply this technique to various materials. There are benefits to this technique that offset the high capital investment including focusability, high power intensity, and ease of automation with in-process sensing [11]. Early testing by

preheating Ti-64 alloys through furnace, plasma, and other methods have found limited success due to excessive heating of the bulk material which may cause part distortion and adverse heat-affected zones [12]. However, it has been shown that localized heating, and specifically through laser-assisted machining (LAM), tool life can be increased for many difficult to machine materials, such as Waspaloy [13], fiber reinforced Al-2 % Cu metal matrix composite [14], titanium [15, 16], and Inconel 718 [17].

Challenges are introduced when attempting to use these laser-assisted techniques to machining Ti-64. Titanium alloys are categorized based on their microstructure and are divided into three main groups: α-alloys, β-alloys, and α/β-alloys. Among the alloys, Ti-64 belongs to the α/β-alloy group which is known for its heat treatability and relatively low Young's modulus. This heat treatability introduces additional challenges when performing laser-assisted material processing.

Experimental results for turning a Ti-64 alloy has shown that tool life can be improved during machining using LAM [15]. The study investigated simultaneous use of liquid nitrogen to cool the tool and a laser to heat the workpiece material to improve machinability. The study showed that cutting force was reduced with laser application and the cutting force could be reduced by 33 % using LAM. The hybrid machining technique of using laser heating of the workpiece and cryogenic cooling of the cutting tool could improve tool life by twofold up to speeds of 150 m/min, while LAM alone produced an improvement in tool life of 1.7 times for speeds below 100 m/min. Analysis of the final workpiece showed that laser parameters could be used, which would not alter final material properties compared with traditional turning.

Work performed by Rahman Rashid et al. [16] investigated the influence of laser power on LAM of Ti-6Cr-5Mo-5V-4A. It was determined that for slow cutting speeds, cutting force could be reduced by LAM to a half of the amount measured during conventional machining. However, as machining speed was increased, the reduction in cutting force was reduced, and there was no significant cutting force reduction beyond cutting speeds of 175 m/min. Their study also showed that both LAM and traditional machining resulted in a change from continuous chips to segmented saw-tooth chips at speeds close to 50 m/min.

The turning process is limited to producing axisymmetric part shapes. On the other hand, milling can produce many complex parts with arbitrary geometry. The differences between turning and milling give rise to potential challenges to laser-assisted milling, which require further investigation. Due to the interrupted nature of milling, recent studies have been performed to determine how laser-assisted milling (LAML) can be implemented to improve machinability.

Shelton and Shin [18, 19] carried out laser-assisted micro-milling on difficult to machine materials of AISI 316, AISI 422, Ti-6Al-4V, and Inconel 718 using side milling and slotting configurations. Improvements were found for surface finish on the final workpiece along with a reduction of edge burrs and a reduction in cutting force as indicated by AE sensor readings. This study showed the feasibility and general improvement that LAML could provide when machining these materials.

Wiedenmann et al. [20, 21] presented temperature prediction work and experimental testing using a laser-assisted face milling setup. Modeling work was used to predict temperatures within the workpiece during the LAML process for a Ti-64 alloy. Modeling included a regression analysis of cutting force in terms of several machining factors such as feed, laser power, and laser lead. Regression analysis showed that the best results in cutting force reduction could be achieved by the use of higher laser power and smaller laser lead distance. A numerical database for predicting a heat-affected zone was created based on the modeling work and experimentally validated using optical inspection of machined workpiece cross-sections. Brecher et al. [22] integrated a laser into a milling machine spindle and performed LAML experiments on an Inconel 718 workpiece. Through coordination of laser heating during tool rotation and workpiece interaction, cutting force was reduced. After machining was performed over a set amount of time, using both LAML and traditional methods, a comparison of flank wear showed that overall tool life was improved with the use of LAML. Ding et al. [23] performed a detailed analysis of the thermal and mechanical processes that occur during laser-assisted micro-milling of 422 SS, Inconel 718, and Ti-64 in a side milling configuration. Modeling was performed to predict cutting forces during machining where a good agreement was found with experimental results. It was determined that LAML successfully reduced the tool wear rate from 0.73 to 0.12 μm/min for side cutting of a 422SS fin-shaped structure.

Sun et al. [24] presented experimental work on LAML of a Ti-64 alloy using up-milling. Basic temperature prediction was performed to determine the temperature of the workpiece at a point on the top surface, and the depth of cut, during the laser heating process. They showed that as laser power was increased, the cutting force in the feed direction decreased. Tool life comparisons by the machining tests showed that LAML produced less wear than traditional milling, but that high laser power would result in melting of the workpiece surface, which would produce chipping of the insert as the tool interacted with this material.

LAML is investigated in this study for machining of Ti-64 grade 5 to determine how machining speed can be improved and machining costs can be reduced. Multiple tool wear tests were performed using a face milling configuration, and tool wear progression is experimentally investigated. Modeling work is performed initially to determine laser parameters that will not produce a heat-affected zone in the final workpiece for a material that is heat treatable. Although similar modeling was performed to predict when a heat-affected zone will appear on the workpiece surface [21], the current modeling work

focuses on determining laser parameters that will avoid such damage, and characterizing the potential benefits of LAML when laser power is limited below a threshold for phase change of the material. A detailed surface integrity analysis is performed on the machined workpiece to determine the influence of laser heating on final part properties. This analysis includes optical and scanning electron microscopy (SEM) images, hardness testing, and residual stress analysis. An economic analysis is also performed for laser-assisted milling to characterize the improvements to final cost per part for LAML and traditional machining.

2 Experimental procedure

Milling experiments were performed on a MAZAK VQC-40/15 vertical milling center with a MAZATROL-M32 controller. The machine has a maximum spindle speed of 6000 RPM and maximum power of 7.5 HP. An IPG Photonics Ytterbium laser system: YLS-1000 was used, which produces a 1.071-μm wavelength laser beam with a maximum power output of 1.0 kW. The focal length of the lens was 401 mm where the focal point was located on the material surface, and the final spot size was 2.6×3.6 mm in an elliptical shape with a Gaussian distribution. The laser was applied at ~44° from normal which resulted in the elliptical shape. The laser lead distance was defined as the distance between the edge of the tool and edge of the laser spot. The overall machining setup is shown in Fig. 1.

A Kennametal Mill 1–14 tool holder (Kennametal M1D075E1402W075L175) with TiAlN-coated carbide grade inserts (KC520) was used during machining tests with a Ti-64 workpiece. The combined geometry of the tool and insert results in a 19.05-mm diameter, 0° lead angle, 15° radial rake, 3° axial rake, and a nose radius of 0.8 mm for the cutting tool. Single insert fly cutting was used during all tool wear and force tests to avoid potential issues with runout. Downmilling was used in all titanium machining experiments with a face milling configuration. A flood coolant was applied during traditional machining experiments, which consisted of a 10 % mixture of oil and water. An assist gas of argon was used in LAML to keep the chips away from the laser delivery optics, and reduce the possibility of fire within the experimental setup.

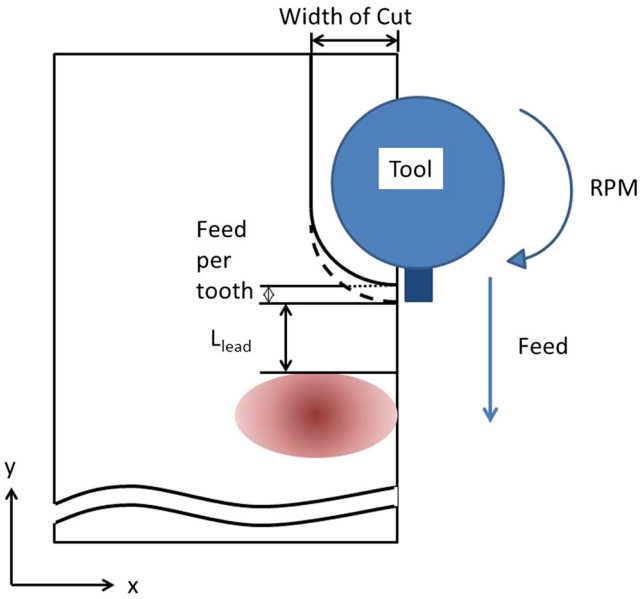

Fig. 1 General machining setup for LAML (*top view*)

A Kistler 3 component dynamometer type 9257B with a Kistler 5004 dual mode amplifier was used to measure cutting force data. Labview software was used to collect data from the amplifier with a sampling rate of 2 kHz during machining of Ti-64. Tool wear measurements were taken using a Nikon Eclipse LV150 optical microscope and analyzed using a SPOT Insight Firewire software and camera.

For microscopic examination, the machined Ti-64 samples were sectioned and prepared using 320, 400, 600, and 800 grit papers and polished using a colloidal silica of 6 and 0.5 μm on a polishing wheel, according to standard metallographic techniques. All samples were etched using Kroll's Reagent (ASTM 192), and images were taken using the Nikon Eclipse LV150 optical microscope and a JEOL T330 SEM.

A Mitutoyo hardness tester (model ATK F1000) was used to determine the surface hardness in the HRC scale using 150 kgf, and a 120° diamond cone indenter. All measurements were taken on the final workpiece surface. Microhardness analysis was performed using a LECO KM 247AT machine, and hardness was recorded using a Vickers hardness scale using a 200-g load and a dwell time of 13 s. Measurements were taken at specific depths below the machined surface to determine the change in hardness with respect to distance. Hardness at a very shallow depth could not be measured accurately as the workpiece would deform when the indenter was too close to the edge.

A Bruker D8 Focus X-Ray Diffractometer was used for X-ray diffraction (XRD) analysis of Ti-64 samples, which has a Cu-K(α) source, a 3-circle goniometer, and a Lynseye 1D detector. A scan step of 0.024° was used with a counting time of 8°/min.

Residual stresses were measured on the Ti-64 samples using the X-ray diffraction technique on Bruker D8 Discover X-Ray Diffractometer with General Area Detector Diffraction System (GADDS) using Cr-K(α) radiation (λ=0.22897 nm) at 30 kV, 50 mA to acquire {103} diffraction peaks at 2θ angles of about 119.3° using a spot of 0.8 mm collimated from the 2 mm beam. A two-dimensional approach was used to evaluate the 2D diffraction data. The data processing and stress evaluation were performed with GADDS software and Materials Data Incorporated's Jade, respectively. Depth profiles for the residual stresses were measured by chemically etching successive layers of the material by electropolishing

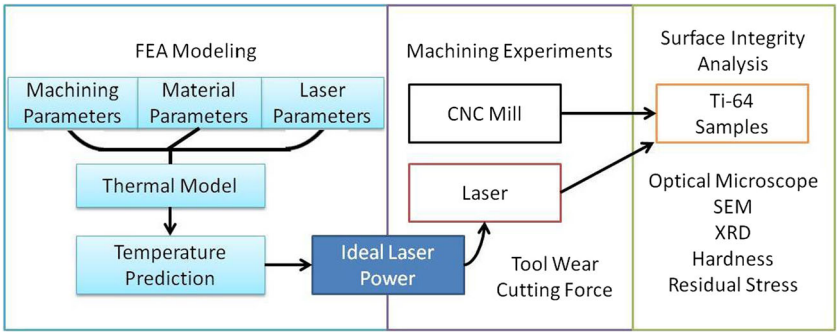

Fig. 2 A flow chart showing the LAML design and characterization procedures

using an etchant of 8 % HF and 92 % H_2O, with an etching interval of 40 s to remove 25 μm of material.

A flowchart illustrating the connections of different phases of this study is given in Fig. 2. Based on the thermal modeling, experimental conditions, particularly laser power according to other cutting parameters, are determined and experiments are designed. Post-machining characterization follows the machining experiments.

3 Thermal model

The temperature distribution in a workpiece undergoing LAML needs to be predicted so that the process can be accurately understood and controlled. A transient, three-dimensional thermal model of a rectangular workpiece undergoing laser heating and material removal was developed at Purdue University and a detailed description, including governing heat transfer equations, boundary conditions, and numerical scheme, is provided by Tian et al. [25].

For the numerical solution, an implicit finite-volume method is used to discretize the governing equation, and the modeled domain is divided into a set of predefined control volumes. A typical $30\times10\times15$ mm^3 workpiece is modeled by a $100\times80\times55$ mesh in the x, y, and z directions, respectively. Modeling of the LAML process was performed using thermal properties for a Ti-64 workpiece, and was simulated for 10 s of machining until a quasi-steady state was established. Laser and tool feed were defined in the x-direction for a face milling configuration. Material removal was enabled, and conduction, convection, and radiation of the material were all considered. It is known from other work [20] that conduction plays the most important role in modeling the LAML process, but convection and radiation were included, since it did not significantly affect computational time. An

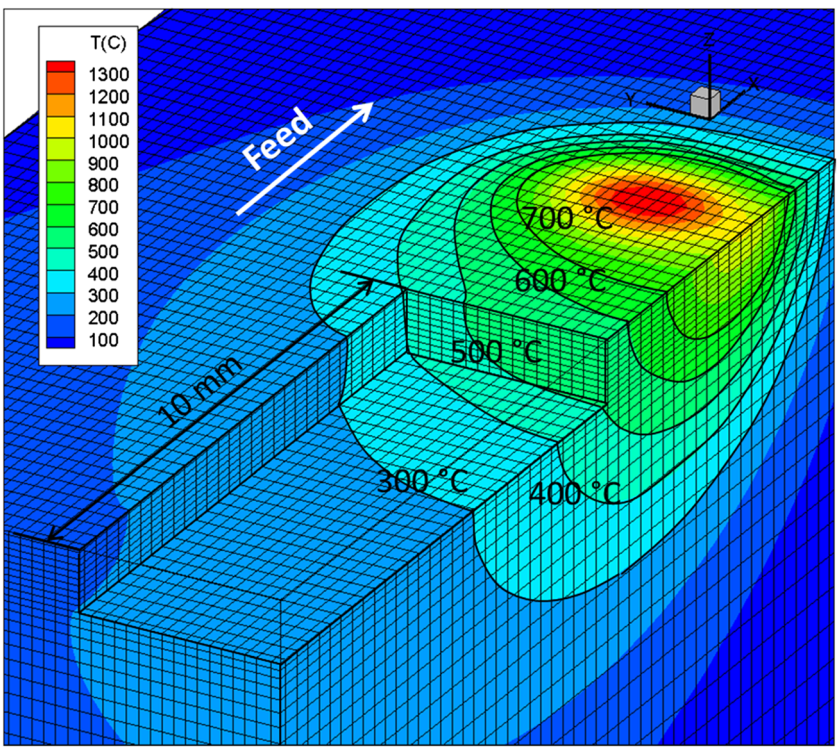

Fig. 3 Example thermal model output for LAML of Ti-64

Table 1 Composition of the workpiece for AMS 4911 specifications

Element	Al	V	Fe	O	C	N	H	Y	Other—total	Ti
Min	5.50	3.50	–	–	–	–	–	–	–	Balance
Max	6.75	4.50	0.30	0.20	0.08	0.05	0.015	0.005	0.4	

example of temperature prediction output from the thermal model is shown in Fig. 3. The model predicts temperature distributions within the workpiece with settings of a 3-mm laser lead distance, a 2.6×3.6 mm elliptical beam shape, 175 W laser power, and 1.2 mm/s feed and included material removal for a 3 mm width of cut.

3.1 Material properties

To obtain an accurate temperature prediction for the workpiece, correct material properties are required. For the experiments performed, the Ti-64 alloy supplied met the AMS 4911 specifications, which is typically used in aerospace applications. Details of the material composition are included in Tables 1 and 2. Material properties were obtained from literature [26, 27], and functions were fitted to the temperature-dependent data for thermal conductivity and specific heat (Table 3). Optical properties of emissivity (0.25) and absorptivity (0.35) for a Ti-64 alloy to an Nd:YAG laser were found from literature [27] and were compared with experimental results for laser absorptivity to the fiber laser. A good agreement was found between the material absorptivity value from literature for a Nd:Yag laser wavelength (absorptivity α= 0.35) with experimental results for workpiece laser absorptivity for a fiber laser wavelength for low laser power, between 40 and 90 W.

It was found that oxidation of the surface became apparent for high laser powers (above 90 W). This was not discussed in the literature, and may not have occurred for experiments in the literature due to a large amount of Argon used. High flow rates for an assist gas onto the workpiece surface are not typical during LAML. During absorptivity testing performed in this study, it was determined that cutting conditions that closely matched LAML parameters resulted in workpiece absorptivity value of 0.5, for the fiber laser and low Argon flow rates. Modeled temperature prediction and IR camera recorded surface temperatures most closely matched for this absorptivity, as shown in Fig. 4.

Table 2 Physical properties of Ti-64 [26, 27]

Density—ρ (kg/m^3)	Young's modulus—E (Pa)	Poisson's ratio	Emissivity	Nd-Yag absorptivity
4430	1.13×10^5	0.34	0.25	0.35

3.2 Modeling results

In order to perform machining experiments using appropriate laser parameters, the thermal model was used to determine a parametric relationship for the average temperature in the material removal zone ($T_{\text{mr-ave}}$), maximum workpiece surface temperature ($T_{\max}$), and maximum temperature on the depth of cut plane (T_{machined}). This was performed by running the model using varying parameters of laser power (P), and feed rate (F). A full factorial design was used to determine temperatures in the areas of interest. MiniTab statistical software was used to perform the multivariable regression analysis to predict workpiece temperatures based on laser and machining parameters. Similar techniques have been used by others to predict workpiece temperatures [15]. This model was subsequently used to ensure that a heat-affected zone was not created in the final workpiece material as a result of laser heating.

The resulting predictive equations from the regression analysis are:

$$T_{\text{mr-ave}} = 32.017 \times \frac{(\alpha P)^{0.772}}{(F)^{0.156}} \tag{1}$$

$$T_{\max} = 133.238 \times \frac{(\alpha P)^{0.633}}{(F)^{0.099}} \tag{2}$$

$$T_{\text{machined}} = 94.492 \times \frac{(\alpha P)^{0.721}}{(F)^{0.23}} \tag{3}$$

with laser power (P) in W, feed rate (F) in mm/min, absorptivity value of 0.5, and temperature (T) in °C. Based on these equations, the laser power was calculated using the feed and appropriate absorptivity, based on the surface temperature expected and experimental cutting conditions. Results from this analysis were used to assist in the selection of appropriate laser power for the laser-assisted milling parameters that would not induce a phase change in the Ti-64 material. As a result of the modeling work, a maximum $T_{\text{mr-ave}}$ of 500 °C was used during experiments to avoid a potential microstructural change on the final surface of the part after machining.

Table 3 Temperature dependent thermal properties for Ti-64 [26]

Property	Equation	Approximation for
Conductivity—k (W/m-K)	$1.00\times10^{-5}\times T^2-0.0012\times T+6.6519$	T (K)>1300 k=22.0
Specific heat—c_p (J/kg-K)	$0.21\times T+483.37$	T (K)>1200 c_p=735

4 Experimental results

4.1 Cutting force

A cutting speed of 50 m/min was used during machining experiments to characterize the influence of laser heating on cutting force, so that an accurate comparison could be made between traditional machining and LAML using a face milling configuration. By reducing cutting force, it is likely that less deformation will occur on the machined components and tool life will be improved by reducing pressure loads on the edge of the tool.

During the machining experiments, cuts were made along a Ti-64 sample with dimensions of $50\times100\times190$ mm^3 and $50\times60\times90$ mm^3 for tool wear and force experiments, respectively, with machining occurring along the longest length. Machining parameters used included a 75 m/min cutting speed, 0.1 mm/tooth feed per insert, 1 mm depth of cut, and 3 mm width of cut. Laser parameters included a 2.6×3.5 mm^2 laser spot diameter, 3.5 mm laser lead distance, and a 41° angle of incidence measured from horizontal.

Tests were performed with and without laser heating of the workpiece, as detailed in Table 4. To avoid potential phase change in the final workpiece surface, a maximum laser power of 180 W was not exceeded during LAML cutting force experiments based on the thermal modeling and regression analysis. It was determined that this power would not increase the temperature at the final depth of cut location beyond the critical cutoff temperature chosen for phase change, which is 800 °C for an area of the workpiece wider than 100 μm. Temperatures for $T_{mr\text{-}ave}$, T_{max}, and $T_{machined}$ were calculated based on the laser parameters used during machining and the regression analysis performed.

Cutting force was recorded at 2 kHz. Examples of measured cutting force data are included in Fig. 5, where Fy is the force in the feed direction and Fx is perpendicular to the feed direction. An example of averaged cutting force data for 4 cycles recorded during experiments is shown in Fig. 5. Peak force data was taken over the total length of cut, and an average peak cutting force was determined for each experiment. It was found that laser heating reduced forces, with the largest reduction of 30 and 50 % in the y and x directions, respectively for LAM5. Figure 6 shows a graphical comparison for the general trend of reduced cutting force for increasing laser power, in addition to the standard deviation of cutting force. From this data, the general trend of decreasing cutting force with increasing laser power can be observed.

The 30 % reduction in cutting force measured during LAML of Ti-64 is not as large as the 60 % reduction observed during milling of Inconel 718 [22] or the 40 % reduction during milling of a Ti-64 alloy [24]. This is mainly a result of differences between laser power and configuration during machining. Because material properties of the final workpiece surface were of critical importance for the Ti-64 alloy, and the material is heat treatable by nature, laser power was limited during LAML experiments. This consideration is not included in the work presented by Brecher et al. [22] and Sun et al. [24]; therefore, with a higher laser power, a larger reduction in cutting force should be expected.

Beam placement can also be a driving factor for the reduction in cutting force. Position of the laser relative to the cutting tool will influence the final temperature profile within the workpiece. As a result, temperatures within the cutting zone can be significantly different, which directly impacts the final cutting force that occurs during machining. For this testing, the more standard approach of applying the laser to the

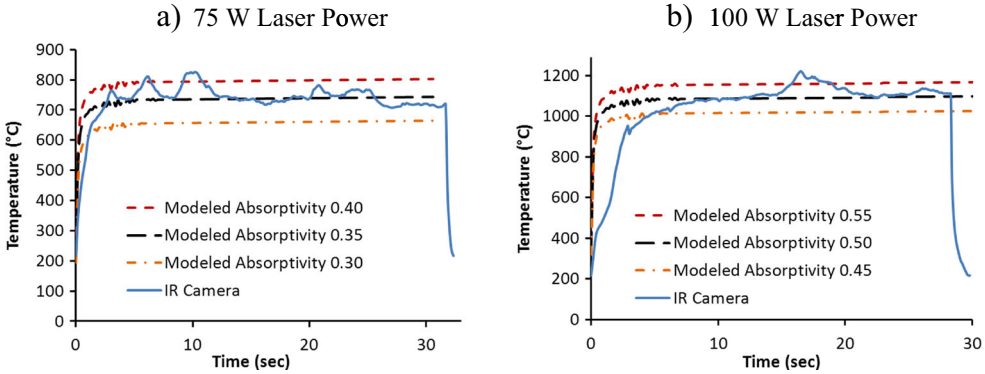

Fig. 4 IR camera results and thermal model calculation to determine workpiece absorptivity

Table 4 Experimental design for LAM of Ti-64

Test	V (m/min)	Feed rate (mm/min)	Feed (mm/tooth)	RPM	P (W)	$T_{mr\text{-}ave}$ (°C)	T_{max} (°C)	$T_{machined}$ (°C)
Conv	50	83.5	0.1	835	0	23	–	–
LAM1	50	83.5	0.1	835	75	200	679	361
LAM2	50	83.5	0.1	835	100	250	815	444
LAM3	50	83.5	0.1	835	127	300	947	527
LAM4	50	83.5	0.1	835	155	350	1075	608
LAM5	50	83.5	0.1	835	170	500	1440	848

workpiece ahead of the cutting tool was used, instead of the novel concept of laser integration through the spindle [22].

4.2 Tool wear

Tool wear tests were performed on the Ti-64 workpiece using TiAlN PVD-coated carbide inserts (Kennametal KC520). Several machining speeds were chosen for this testing to determine total tool life for traditional milling and LAML, to establish a baseline for overall tool life. Traditional milling using a flood coolant found that cutting speeds above 50 m/min would result in premature chipping of the tool during Ti-64 machining. This chipping can occur on the flank or face of the insert, and reduces the predictability of tool life. Chipping is quite common when machining titanium alloys and limits the cutting speed to 50 m/min and lower in industry.

It is recommended by ISO 8688–1 that the tool should be rejected when the depth of chipping on the flank face or the width of chipping on the rake face are greater than 0.25 mm. To prevent potential damage to the experimental equipment, total flank wear greater than 220 μm from the edge of the initial tool geometry was used in this study to define total tool life.

LAML experiments were performed on the Ti64 workpiece using the highest machining speed possible for conventional machining (50 m/min), as well as higher cutting speeds up to 75 m/min. LAML testing was performed using an argon gas to prevent chips from either entering the laser optics or adhering to the cutting tool during machining. A total flow rate of 0.47 lpm at 0.35 MPa was delivered using two nozzles. A concise summary of machining parameters for traditional milling and LAML is included in Table 5.

Machining was performed for a set amount of time for each machining speed with tool wear recorded for total flank wear observed on the insert (Fig. 7). Based on tool life testing at 37 m/min using traditional machining with a flood coolant, an equivalent tool life was achieved using LAML without a coolant at a cutting speed of 50 m/min. As a result, cutting speed can be increased by 35 % for LAML of Ti-64 grade 5, where the tool will spend the same amount of time removing material before it needs to be replaced. This potential increase of 35 % in cutting speed was observed at higher cutting speeds, when comparing traditional milling with LAML. If an increase in cutting speed is not required, LAML can remove 35 % more material than traditional milling over time before the tool must be replaced.

From Brecher et al. [22], it was found that LAML of Inconel 718 resulted in significantly reduced cutting force and tool wear. During machining tests at 75 m/min, using 1000 mm^3 of removed material, 140 and 60 μm of flank wear were present for traditional machining and LAML, respectively. This is significantly better than the results of the current work; however, laser power considerations must be taken into effect. Inconel 718 is not a heat-treatable material, and hence, a much higher laser power could be employed during their study. As a result, much

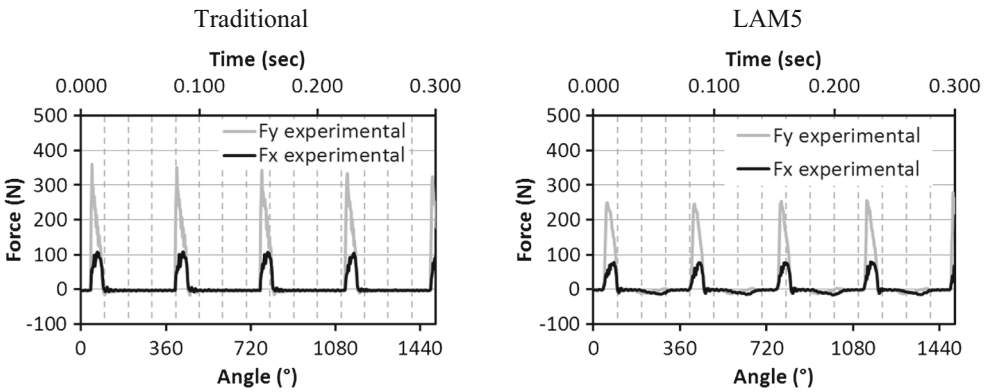

Fig. 5 Experimental cutting force during multiple tool rotations

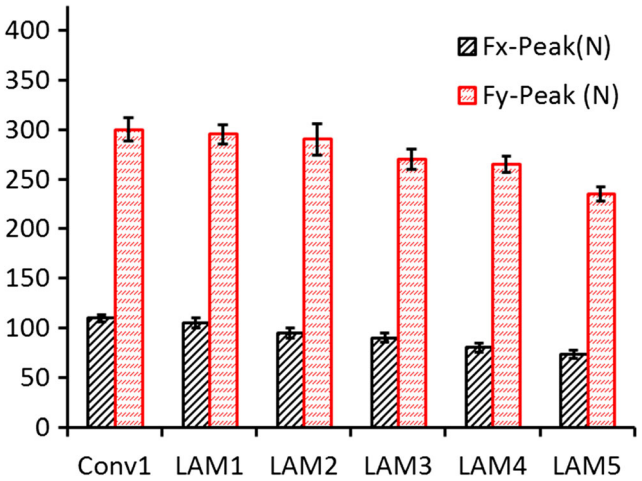

Fig. 6 Average peak cutting force results—*error bars* for one standard deviation of 50 cycles

larger cutting force reduction and improvement in tool life could be achieved during LAML of Inconel 718. It must be noted that laser parameters used in this study are not necessarily optimal because the study focused on tool life testing. It is conceivable that greater tool life improvements may be achievable through a modification of laser parameters including spot size, lead distance, laser power, and beam placement.

To compare overall tool life for traditional milling and LAML, the Taylor tool life equation was used to characterize failure of the tool as a result of flank wear. Failure of the tool was defined by flank wear that had exceeded 220 μm for a predictable tool life at all cutting conditions, without premature chipping. Using this criterion, a Taylor tool life equation was determined for both traditional milling and LAML of Ti64:

$$\text{Conv}-V_c \times T^{0.225} = 112 \tag{4}$$

$$\text{LAM}-V_c \times T^{0.299} = 208 \tag{5}$$

Table 5 Tool wear—experimental parameters

Test	V (m/min)	RPM	Feed (mmpt)	P (W)	$T_{\text{mr-ave}}$ (°C)	Coolant
Conv-A	37	618	0.1	–	CONV	Oil-based
Conv-B	45	752	0.1	–	CONV	Oil-based
Conv-C	50	835	0.1	–	CONV	Oil-based
Conv-D	50	835	0.1	–	CONV	Oil-based
LAML-A	50	835	0.1	170	500	None
LAML-B	60	1003	0.1	175	500	None
LAML-C	75	1253	0.1	185	500	None

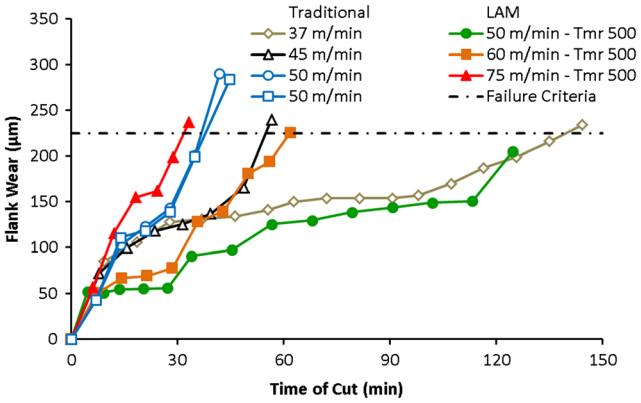

Fig. 7 Ti-64 tool wear—520 insert

4.3 Microstructural analysis

It is essential that the final workpiece surface of Ti-64 grade 5 be characterized to identify changes in properties that can occur during machining. Due to the addition of heat from the laser to the workpiece surface, a heat-affected zone can potentially be created on the finished part. Although modeling was performed to obtain an appropriate laser power based on material properties, machining parameters, and laser parameters, additional analysis must be conducted to ensure that final workpiece properties were not significantly altered during the LAML process.

4.4 Optical microscope comparison

Images were taken using an optical microscope from samples machined using Conv-C at 50 m/min and LAML-C at 75 m/min for tool life experiments, which were then cross-sectioned and prepared using standard metallographic techniques. A comparison of grain size and orientation beneath the machined surface was performed to determine what influence LAML had on final part microstructure. Based on observations of the cross-sectioned samples (Fig. 8), it was found that there was no difference in grain size directly below the machined surface of any of the samples, and that the samples were similar down to a deep depth (>2 mm). Grain orientation appeared to be random, with no specific orientation resulting from machining. Overall, no significant difference was observed between the two types of machining when optically comparing microstructures of the machined sample cross-sections. As in the case of Wiedenmann et al. [20], modeling was successful to avoid a heat-affected zone on the final workpiece surface after LAML.

4.5 SEM analysis

SEM images were taken and compared between traditional milling and LAML cross-sectioned samples in order to make a better comparison of grain size and orientation of the Ti-64

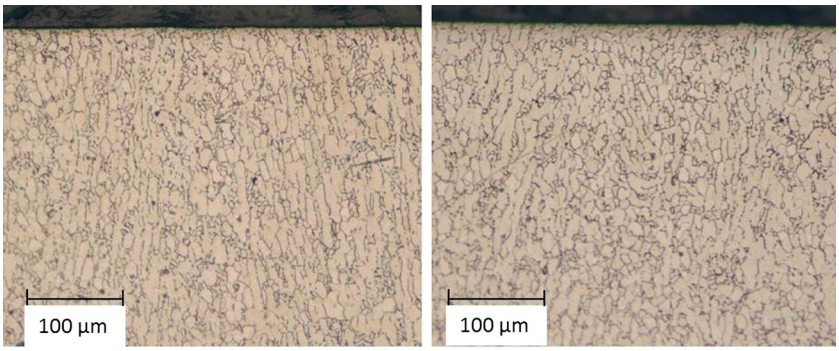

Fig. 8 Ti-64 optical microscope images from cross-sectioned samples etched with Kroll's reagent at ×200 after traditional machining (**a**) and LAML (**b**)

samples. The SEM images obtained are consistent with other images from literature [28] for an AMS 4911 plate of Ti-64 grade 5. From a microstructural comparison, it was found that there is no clear difference in grain boundaries between the two cases for the α-phase present, and that a microstructure of equiaxed α with a small amount of intergranular β is present through the entirety of the part (Fig. 9). By observing the cross-section of the material, it was determined that there was not a significant change in material composition from the top of the machined surface all the way to the bulk of the material (>2 mm). As a result of optical microscope and SEM images, it can be concluded that the LAML process parameters chosen did not produce a heat-affected zone in the final workpiece.

4.6 XRD analysis

Because Ti-64 is a heat-treatable alloy, material properties of the workpiece can change when it is irradiated by a laser. For cases without material removal, a laser has been used successfully to change an α-phase Ti workpiece with a small amount of β-phase into a predominantly β-phase Ti with a small amount of α-phase in the areas of the workpiece under laser irradiation [29]. Such phase changes can be beneficial, or detrimental to the final workpiece, depending on the specific needs of a component. To generally characterize the improvement that can be achieved during LAML, and based on the specifications for an AMS 4911 plate which is provided in an annealed state, it was assumed that a phase change on the final workpiece would have a detrimental impact on final part properties. Laser power levels were limited to ensure that temperatures did not exceed the critical cutoff for phase change based on the maximum temperatures predicted by thermal modeling.

Although optical images and SEM images indicate that there is no significant microstructural change, non-destructive XRD analysis was performed on the top workpiece surface to ensure that phase change was avoided for this critical area. Samples did not receive special preparation and had an average surface roughness of 0.3 µm. From literature [30–32], the standard way to characterize the 2θ peaks in Ti-64 is to use the Joint Committee on Powder Diffraction Standards (JCPDS) for titanium. The hexagonal α-Ti, and cubic β-Ti from the JCPDS (file #44-1294, and #44-1288, respectively) were used to determine where peaks should occur. This analysis is plotted along with the XRD experimental data (Fig. 10).

From a comparison of measured peaks to reference points, it can be seen that the machined surface mainly consists of α-phase Ti after traditional machining. Since there are no significant peaks present for the β-phase Ti on the LAML sample, it can be concluded that machining with the laser will not induce a phase change, as long as appropriate laser power is used to perform LAML. This indicates that thermal model predictions can be used to accurately determine maximum laser power to

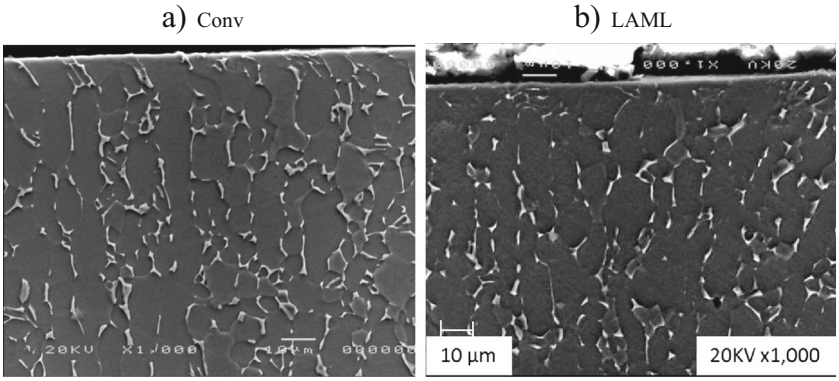

Fig. 9 SEM images of etched Ti64 sample at ×1000 after traditional machining (**a**) and LAML (**b**)

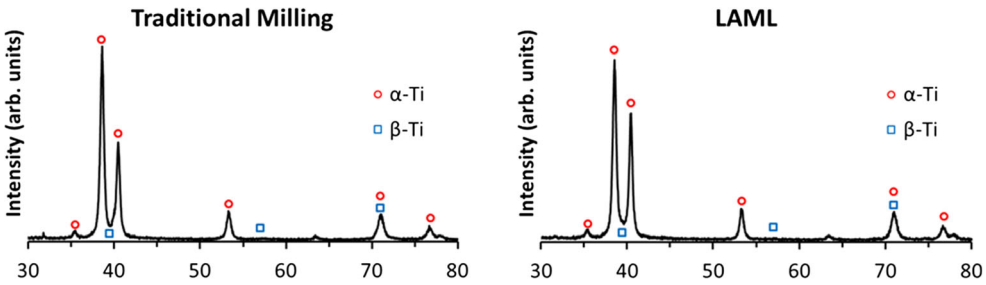

Fig. 10 XRD analysis for milling Ti-64

enhance machining of the material, without exceeding the critical threshold temperature for Ti-64 grade 5 during LAML. This conclusion is reinforced through the images from the SEM, which show no significant change in grain size and orientation at the machined surface as well as within the bulk material.

4.7 Material hardness

A Mitutoyo hardness tester (model ATK F1000) was used to determine the overall surface hardness of the original Ti-64 material, samples after traditional machining, and samples machined using LAML. Each sample was tested eight times and the results are included in Fig. 11. The error bars included are for one standard deviation of the measured data.

From these measurements, it was determined that there is a very slight decrease in the surface hardness of the final part. However, this is not a result of a detrimental phase change, based on the XRD analysis performed. During traditional machining, there can be an increase in surface hardness from grain size refinement and increased residual stresses during plastic deformation and the shearing process. It has been shown that compressive residual stresses are generally observed during the milling of titanium [33]. This increase in compressive residual stress can result in an adverse reduction of ductility at the surface of the part.

The measured surface hardness was reduced by less than 10 % for the LAML samples when compared with traditional machining. As a result, final hardness measurements were within the range of the as-received material for hardness.

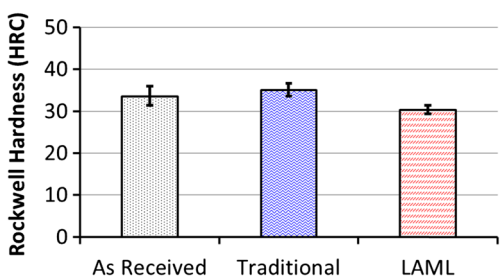

Fig. 11 Ti-64 surface hardness results for the as-received material, traditional milling at 50 m/min, and LAML at 75 m/min (*error bars* for the range of data)

The overall measured variations of final surface hardness for both types of machining were greatly reduced, when compared with those of the as-received material.

Due to the measured reduction in surface hardness, a detailed investigation into microhardness was performed to determine if there was a significant alteration in hardness beneath the surface of the LAML workpiece. Microhardness analysis was performed on cross-sectioned samples for Conv-C at 50 m/min and LAML-C at 75 m/min using a LECO KM 247AT machine.

Microhardness was analyzed at intervals of 100 μm for each sample down to a depth of 2 mm, with an additional data point at 50 μm. Hardness closer to the workpiece surface could not be measured accurately, as the workpiece would deform when the indenter was too close to the edge.

It was determined that there was a relatively consistent hardness for both LAML and traditional machining, and that this hardness did not significantly change through the depth of the workpiece. Close to the surface of the workpiece, a gradual increase in hardness was observed for both LAML and traditional machining, indicating that the surface hardness differences measured were very shallow with respect to the top of the workpiece surface (Fig. 12). Significantly, there was not a detrimental decrease in hardness of the workpiece as a result of LAML when compared with the bulk workpiece material, and surface hardness measurements fell within the acceptable range for Ti-64 grade 5 based on AMS 4911 specifications.

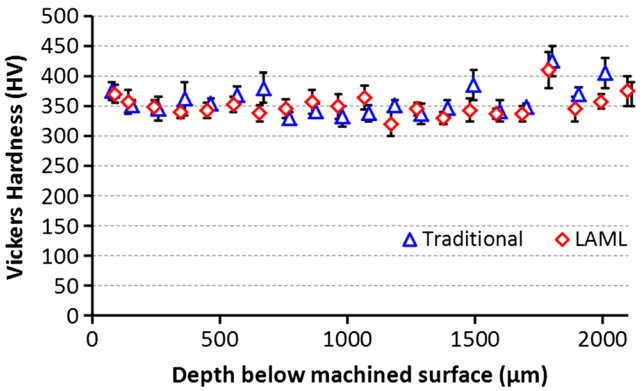

Fig. 12 Microhardness results for traditional machining at 50 m/min and LAML at 75 m/min

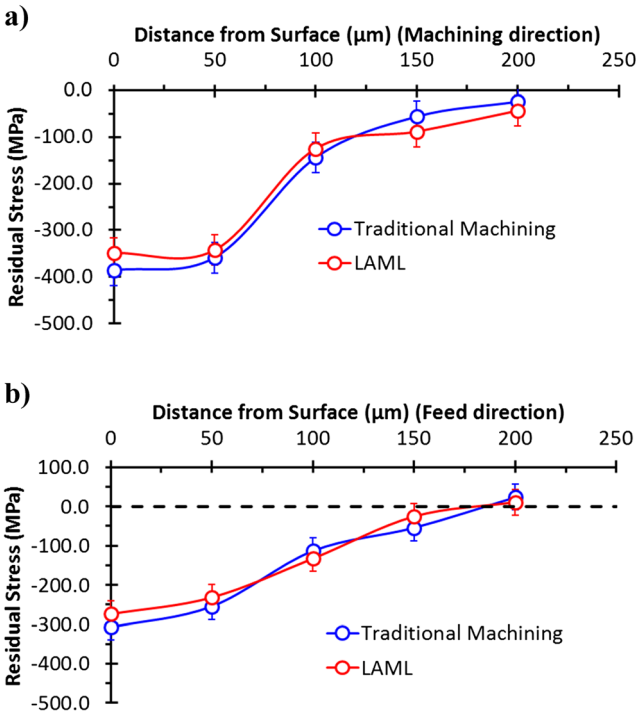

Fig. 13 Residual stress measurement for Ti-64 after traditional machining at 50 m/min and LAML at 75 m/min for the machining direction (**a**) and feed direction (**b**)

4.8 Residual stress

Residual stress analysis was performed on the machined samples for Conv-C at 50 m/min and LAML-C at 75 m/min. Measurements were taken from the machined surface of the sample in the feed and machining direction. The surface was etched and additional residual stress measurements were taken to a depth of 200 μm where stresses returned to zero.

It was found that there was a slight reduction in compressive residual stress on the surface of the workpiece as a result of the different machining processes. The reduction from LAML was close to 10 % in both 2D directions, which is consistent with the measured results of final workpiece surface hardness. Comparisons of residual stress data for traditional milling and LAML in the machining and feed directions are included in Fig. 13.

When comparing the results of the residual stress with surface hardness and microhardness measurements, it is clear that LAML induces less residual stress onto the workpiece during machining, resulting in a slight decrease in surface hardness. This is perhaps due to the reduction in cutting force, or stresses induced during LAML. The reduced residual stress only affects a very shallow portion of the machined workpiece and does not affect workpiece properties at deeper depths (below 200 μm).

From all of the microstructural analysis performed on the final workpiece, it can be concluded that LAML machining parameters can be implemented such that they do not negatively influence final workpiece properties. Laser parameters can be calculated prior to machining using thermal modeling predictions for a workpiece. This allows the process to increase tool life and machining speeds while avoiding negative effects of laser heating during the LAML process. It was also determined that LAML allows for the implementation of higher machining speeds without affecting final part properties.

4.9 Ti-64 economic analysis

To characterize the benefits that result from LAML, an economic analysis was performed for both traditional milling and LAML based on tool life predictions using the following equation:

$$\text{Cost} = CT \times C_o + \frac{C_t \times CT}{T} + \frac{T_c \times C_o \times CT}{T}$$

where C_o is operating cost ($/min), CT is cutting time (min), T is tool life (min), C_t is initial tool cost ($), and T_c is tool changing time (min). Cost savings can be calculated for the increase in tool life achievable in LAML. The analysis uses the following assumptions for operating conditions and associated costs:

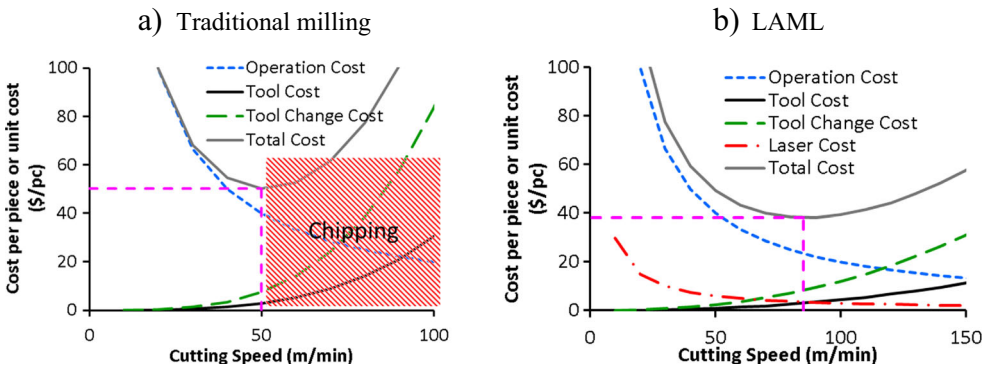

Fig. 14 Cost of producing one part based on Taylor tool life equations

Table 6 Optimized cutting speed based on Taylor tool life equations—Ti-64 milling

Machining type	Optimized cutting speed	
	Min-cost (m/min)	Max-productivity (m/min)
Traditional	50	54
LAML	85	90

- $200 per hour operation cost rate
- 7 min tool change time
- Tool cost $17 per insert—2 cutting sides ($8.50 per tip)
- Part size 4000 mm^3 (amount of material removed per part)
- At least one part made per tool
- Laser costs $30 per hour for operation and depreciation

Laser costs were estimated based on an initial investment of $1.7 million and used a linear depreciation over 10 years with no residual value. An additional $10 per hour was also assumed for a laser-certified CNC operator.

From the assumptions given and the Taylor tool life equations obtained from experimental testing, the total cost per piece was plotted for different cutting speeds during traditional machining with a coolant and LAML (Fig. 14). Since premature chipping does not occur during LAML, higher cutting speeds are possible for part fabrication. As a result, LAML can be performed at speeds that are optimized based on total machining costs.

The optimum cutting speed to minimize cost and maximize productivity was calculated for both traditional machining and LAML (Table 6). These values were determined by balancing material removal rate and tool life to produce the lowest cost per part, or maximum part production. The calculated total cost for traditional machining using a cutting speed of 50 m/min is highlighted in Fig. 14a with premature chipping occurring at cutting speeds above 50 m/min, as indicated. The minimum cost for LAML is highlighted in Fig. 14b. The potential increase in machining speed can be clearly seen when comparing the two charts, and a reduction in cost per piece is also observed.

The total machining cost for machining one part is calculated for the optimum cutting conditions, with costs separated into their sources (laser, tool change, tool cost, and operational cost) as shown in Fig. 15. As evidenced in the table, there is a 33 % reduction in cost for producing parts using LAML, even when accounting for the costs of the laser operation. Laser operational costs include powering the laser and chiller, supplying an assist gas, and depreciation of equipment over time.

One significant benefit of LAML over traditional milling, which is not considered in this economic analysis, is the impact of a coolant during machining. Since LAML does not require traditional coolants during the machining process, there can be added economic savings. There is also a direct environmental impact from the elimination of coolants since they do not need to be processed after they are no longer useful. It should be noted that there are additional safety benefits provided to the operator of the equipment when a coolant is not used; however, it is recognized that safety precautions are needed for successful implementation of LAML.

5 Conclusions

Laser-assisted milling was investigated to determine what benefits can be gained when machining a Ti-64 workpiece. Testing was performed using constrained machining and laser parameters based on material properties. Initial thermal modeling predicted workpiece temperatures during the process and were used to define laser parameters for the experiments performed. Cutting force experiments showed a 30 and 50 % decrease in cutting force in the feed and machining direction, respectively. It was determined that LAML produced less flank wear at similar speeds to traditional machining, and also found that LAML could be used at higher cutting speeds without inducing premature tool chipping, which limits traditional machining speeds. It was determined that the cutting speed can be increased by 30 % when using LAML

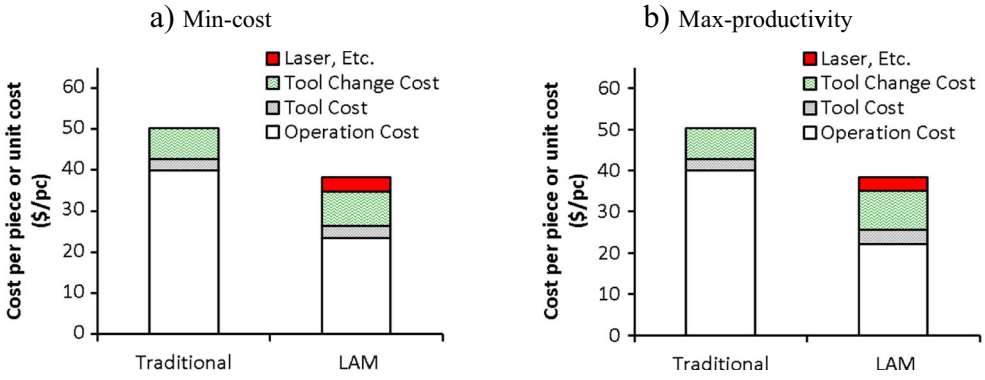

Fig. 15 Economic summary for optimized cutting conditions—Ti-64 machining

compared with traditional milling without reducing the total tool life of the insert.

Optical and SEM images showed that a negative heat-affected zone was not produced, and XRD analysis found that there was not a detrimental phase change present on the finished workpiece surface. Hardness testing found a small decrease in surface hardness for the workpieces, but microhardness analysis showed that hardness did not significantly change through the depth of the workpiece. Residual stress analysis showed a 10 % decrease in compressive residual stress was present for LAML parts compared with traditional machining. The decrease in compressive residual stress measured on the LAML workpiece did not influence workpiece properties of the bulk material and was limited to a shallow layer on the top workpiece surface that was machined. The differences in surface hardness and residual stress can be directly linked to the heat treatability of the Ti-64 workpiece.

An economic analysis showed that despite the increased cost of laser equipment and operation, a significant reduction in cost per part and an improvement in material removal rate can be achieved with LAML. Cutting speeds which are limited to 50 m/min in traditional milling can be increased to 85 m/min for LAML, and a 33 % reduction in cost can be achieved, despite the additional cost of laser equipment.

Future work should investigate the influence of modifying laser parameters and tool types to optimize total tool performance. Additional work can also be done to study how different machining configurations can be implemented and how such changes can improve machinability of advanced materials.

Acknowledgments The authors wish to gratefully acknowledge the financial support provided by the Boeing Company and their approval for publication of this work.

Compliance with ethical standards The authors hereby confirm that there is no potential conflict of interest, and the research did not involve any human participants and/or animals. The authors also consent to the content and publication of this work.

References

1. Boyer, R., Gerhard, W., Collings, E. W., (1994) Material properties handbook titanium alloys, ASM International, pp. 483–485
2. Donachie M. J. (1988) Titanium: a technical guide, ASM International, Second Ed., pp. 6–11
3. Komanduri, R. and Reed, Jr., W.R. (1983) Cutting insert with means for simultaneously removing a plurality of chips", US patent US4552492 A
4. Kuljanic E, Fioretti M, Beltrame L, Miani F (1998) Milling titanium compressor blades with PCD cutter. CIRP Ann Manuf Technol 47(1): 61–64
5. Jawaid A, Sharif S, Koksal S (2000) Evaluation of wear mechanisms of coated carbide tools when face milling titanium alloy. J Mater Process Technol 99(1–3):266–274
6. López de Lacalle LN, Pérez-Bilbatua J, Sánchez JA, Llorente JI, Gutiérrez A, Albóniga J (2000) Using high pressure coolant in the drilling and turning of low machinability alloys. Int J Adv Manuf Technol 16(2):85–91
7. Ezugwu EO, Da Silva RB, Bonney J, Machado ÁR (2005) Evaluation of the performance of CBN tools when turning Ti–6Al–4V alloy with high pressure coolant supplies. Int J Mach Tools Manuf 45(9):1009–1014
8. Rahim, E. A., Sasahara, H. (2010) "High speed MQL drilling of titanium alloy using synthetic ester and palm oil," Proceedings of the 36th International MATADOR Conference, pp. 193–196
9. Sun J, Wong YS, Rahman M, Wang ZG, Neo KS, Tan CH, Onozuka H (2006) Effects of coolant supply methods and cutting conditions on tool life in end milling titanium alloy. Mach Sci Technol Int J 10(3): 355–370
10. Su Y, He N, Li L, Li XL (2006) An experimental investigation of effects of cooling/lubrication conditions on tool wear in high-speed end milling of Ti-6Al-4V. Wear 261(7–8):760–766
11. Steen W (2003) Laser material processing, 3rd edn. Springer, New York
12. Sun S, Brandt M, Dargusch MS (2010) Thermally enhanced machining of hard-to-machine materials—a review. Int J Mach Tools Manuf 50(8):663–680
13. Ding H, Shin YC (2013) Improvement of machinability of Waspaloy via laser-assisted machining. Int J Adv Manuf Technol 17(2):246–269
14. Dandekar C, Shin YC (2010) Laser-assisted machining of a fiber reinforced Al–2 % Cu metal matrix composite. Trans ASME J Manuf Sci Eng 132(6):061004
15. Dandekar C, Shin YC (2010) Machinability improvement of Ti6Al4V alloy via LAM and hybrid machining. Int J Mach Tools Manuf 50(2):174–182
16. Rahman Rashid RA, Sun S, Wang G, Dargusch MS (2012) The effect of laser power on the machinability of the Ti-6Cr-5Mo-5V-4Al beta titanium alloy during laser assisted machining. Int J Mach Tools Manuf 63:41–43
17. Anderson M, Patwa R, Shin YC (2006) Laser-assisted machining of Inconel 718 with an economic analysis. Int J Mach Tools Manuf 46: 1879–1891
18. Shelton JA, Shin YC (2010) Laser-assisted micro-milling of difficult-to-machine materials in a side cutting configuration. J Micromech Microeng 20(7):075012
19. Shelton JA, Shin YC (2010) Experimental evaluation of laser-assisted micro-milling in a slotting configuration. Trans ASME J Manuf Sci Eng 132(2):021008
20. Wiedenmann R, Langhorst M, Zaeh MF (2011) Computerized optimization of the process parameters in laser-assisted milling. Lasers Manuf 2011 Proc Sixth Int WLT Conf Lasers Manuf 12(A):607–616
21. Wiedenmann R, Liebl S, Zaeh MF (2012) Influencing factors and workpiece's microstructure in laser-assisted milling of titanium. Laser Ass Net Shape Eng 7 39:265–276
22. Brecher C, Rosen C, Emonts M (2010) Laser-assisted milling of advanced materials. Phys Procedia 5(B):259–272
23. Ding H, Shen N, Shin YC (2012) Thermal and mechanical modeling analysis of laser-assisted micro-milling of difficult-to-machine alloys. Micro-Manuf Process 212(3):601–613
24. Sun S, Brandt M, Barnes JE, Dargusch MS (2011) Experimental investigation of cutting forces and tool wear during laser-assisted milling of Ti-6Al-4V alloy. Proc Inst Mech Eng B J Eng Manuf 225(9):1512–1527
25. Tian Y, Wu BX, Shin YC (2008) Laser-assisted milling of silicon nitride and Inconel 718. ASME J Manuf Sci Eng 130(3):031013
26. Touloukian YS (1970) Thermophysical Properties Research Center, Purdue University, thermophysical properties of matter; [the TPRC

data series; a comprehensive compilation of data]. IFI/Plenum, New York
27. Yang J, Sun S, Brandt M, Yan W (2010) Experimental investigation and 3D finite element prediction of the heat affected zone during laser assisted machining of Ti6Al4V alloy. J Mater Process Technol 210(15):2215–2222
28. Chandler HW (1989) Machining of Reactive Metals. ASM Handbook - Machining 10:844–857
29. Hahn JD, Shin YC, Krane MJM (2007) Laser transformation hardening of Ti-6Al-4V in solid state with accompanying kinetic model. Surf Eng 23(2):78–82
30. Vreeling JA, Ocelík V, De Hosson JTM (2002) Ti–6Al–4V strengthened by laser melt injection of WCp particles. Acta Mater 50(19): 4913–4924
31. Güleryüz H, Çimenoğlu H (2004) Effect of thermal oxidation on corrosion and corrosion–wear behaviour of a Ti-6Al-4V alloy. Biomaterials 25(16):3325–3333
32. da Silva SLR, Kerber LO, Amaral L, dos Santos CA (1999) X-ray diffraction measurements of plasma-nitrided Ti–6Al–4V. Surf Coat Technol 116–119:342–346
33. Mantle AL, Aspinwall DK (2001) Surface integrity of a high speed milled gamma titanium aluminide. J Mater Process Technol 118:143–150